ADVANCED MATERIALS TECHNOLOGIES
www.advmattechnol.de

Liquid-Metal-Based Soft Pressure Sensor and Multidirectional Detection by Machine Learning

Osman Gul, Jeongnam Kim, Kyuyoung Kim, Hye Jin Kim, and Inkyu Park**

Electronic skin (e-skin) is an emerging technology with promising applications in various fields, including human–machine interfaces, prosthetics, and robotics. Soft and flexible sensors are vital components for the e-skin that can mimic human skin's sensing capabilities. Among soft sensors, liquid-metal-based sensors have gained attention owing to their unique properties, such as high electrical conductivity, stretchability, and elasticity. Herein, a novel approach is presented that enables multidirectional pressure sensing with a machine-learning approach from the transient response of the liquid-metal-based soft pressure sensor for the e-skins. In this study, a soft sensor is developed that utilizes liquid metal and has an array of microchannels on a dome-shaped structure to detect pressures from multiple directions. The transient response from six microchannels of the sensor is used as the input for a convolutional neural network (CNN) to predict the direction (classification accuracy of 99.1%) and magnitude (regression error of 20.13%) of the applied pressures in real time. Finally, a potential application of the developed liquid-metal-based soft sensor as a human–machine interface device is demonstrated by using it to control an RC model car through multidirectional predictions (pressure direction and magnitude) through machine learning in real time.

1. Introduction

The human skin is a remarkable organ that plays a crucial role in our perception of the external world[1–3] With the advent of soft robotics, there has been a growing interest in developing electronic skin that can mimic human touch-sensing abilities.[4,5] For electronic skin to be effective, it must be highly flexible and stretchable to adapt to its surroundings.[6] The development of flexible and stretchable soft sensors has gained rapid momentum, as they have a wide range of applications, including human motion monitoring,[7,8] healthcare monitoring,[9–11] and wearable robots.[12] Owing to its advantageous properties, liquid metal has gained substantial utilization in fabricating flexible and soft sensors.[13–17] However, electronic skin needs to be able to sense different types of pressures, such as radial pressures, which require the development of a soft multidirectional pressure sensor.[18–21] The development of soft multidirectional sensors plays a pivotal role in increasing the amount of data captured by an electronic skin. Although previous studies have developed multidirectional pressure sensors, the investigation into discerning the direction and magnitude of applied pressure remains an unexplored domain.[22,23] Soft sensors exhibit hysteresis and nonlinearity, which makes it challenging to implement conventional calibration methods.[24] Multidirectional pressure sensors have been extensively developed in literature owing to their vast application opportunities. Recently, the trend has shifted towards developing soft sensors with a focus on the design of the structure and sensing materials. To achieve this, flexible and stretchable sensing materials have been employed, resulting in various 3D structures with different detection principles. The four-element sensing structure is the most commonly used structure for multidirectional sensors, in which the four sensing elements are positioned at 90-degree intervals from one other, forming cube-like structure. Through the four-element sensing structure, it facilitates measurement of multidirectional forces. Wide-ranged 3D bump structures are used at the top of the sensing materials to identify the applied multiaxial forces. Lee et al. demonstrated trapezoid structure and CNT array as the sensing material.[25] Pyo et al. also demonstrated a multiaxial force sensor case with a 3D dome structure at the top of the multiple NiCr piezoresistive sensors.[26] On the other hand, Jung et al. proposed a multiaxial force sensor with the sensing materials placed on the sidewalls of the 3D bump structure.[27] Vogt et al. and Kim et al. presented liquid-metal-based multiaxial force sensors with rigid pressure transmission structures on the top of the liquid metal channels.[28,29] In these sensors, the multidirectional force is

O. Gul, K. Kim, I. Park
Department of Mechanical Engineering
Korea Advanced Institute of Science and Technology (KAIST)
291 Daehak-ro, Yuseong-gu, Daejeon 34141, Republic of Korea
E-mail: inkyu@kaist.ac.kr
O. Gul, J. Kim, H. J. Kim
Intelligent Components and Sensors Research Section
Electronics and Telecommunication Research Institute (ETRI)
218 Gajeong-ro, Yuseong-gu, Daejeon 34129, Republic of Korea
E-mail: nolawara@etri.re.kr
J. Kim, H. J. Kim
Department of Advanced Device Technology
University of Science and Technology
Daejeon 34113, Republic of Korea

The ORCID identification number(s) for the author(s) of this article can be found under https://doi.org/10.1002/admt.202302134

DOI: 10.1002/admt.202302134

generated by applied shear force to the four-sensing structure of the sensor. Nevertheless, extracting directional information from four-sensing element-based sensors' setup when exposed to applied radial pressure remains a formidable challenge, primarily because this method is primarily designed for shear force related applications.

In this study, we present a new solution to address the limitations of existing multiaxial sensors. Our approach involves the development of a soft sensor using liquid metal with a dome-shaped design that enables discrimination of directional pressures. Additionally, we leverage machine learning algorithms to identify the direction and amount of applied pressure. The microchannels of the soft sensor were created using fused deposition modeling (FDM). A 3D printed mold made of poly(vinyl alcohol) (PVA) was embedded into the elastomer and dissolved with water to create the microchannels. The empty microchannels were filled with liquid metal, and a vacuum process was applied to create the dome structure for multidirectional pressure sensing. The microchannels within the liquid-metal-based soft sensor exhibit a transient response when pressure is applied. Specifically, each direction of the sensor indicates a distinct transient response when the pressure is applied, which helps to differentiate between different directions of applied pressure. The machine learning technique we have implemented is based on dual-task 1D convolutional neural networks (CNN) which allows real-time classification of the directions and regression of the magnitude from the applied multidirectional pressures by their distinct transient responses. The effectiveness of the sensor and algorithm is demonstrated with human–machine interface application where the sensor is used to control an RC model car. The machine learning predictions, including direction and magnitude of the pressure are used to control the vehicle's real-time movement.

2. Results and Discussion

2.1. Description of the Soft Sensor and Multidirectional Detection Strategy

The liquid-metal-based soft sensor consists of two structures: liquid-metal-based microchannel arrays with a multilayered elastomer structure and a soft dome structure. Using the same elastomer material as the multilayered structure ensures that the dome structure is completely soft. Three straight microchannels on the top layer and another three microchannels on the bottom layer were designed in a cross-bar configuration (**Figure 1**a,b). The liquid metal microchannel array was designed for the discrimination of loading direction. The dome structure makes it possible to discriminate various angles of applied pressure (Figure 1c). Throughout this study, multidirectional pressures were employed using an inclined structure (Figure S1, Supporting Information). Thus, a simple matrix-based visualization method is utilized to show applied pressure on each direction. The minimum width of the microchannel was limited to 500 µm in the FDM 3D printing process. The designed sensor structure was confined to three microchannels, aiming to create the smallest possible multidirectional pressure sensor achievable through the FDM 3D printing process. An increase in the number of microchannels will lead to an improved resolution of the proposed multidirectional detection. In our prior study, experiments focused on dome height and sensor sensitivity, revealing that the highest dome structure resulted in wide ranged pressure sensing.[30] Consequently, we selected the maximum achievable dome height through the vacuum application. Conversely, lower dome heights pose challenges in discerning radial directional pressures within a narrow-angle range. Consequently, an increase in dome height undoubtedly expands the radial directional sensing range. As the bottom microchannels and top microchannels are perpendicular to each other, they form three by three matrix for spatial detection of the applied pressures. Furthermore, the liquid-metal-based soft sensor can detect radial pressure when applied in a 360° spatial range with an interval of 45°. Figure 1d demonstrates the machine learning approach used for real-time regression and classification. The sensor response data is divided into segments using a sliding window technique to achieve real-time estimation of direction and magnitude of applied pressure. These segments are combined to create a tensor, which is then processed by a 1D convolutional neural network (CNN) architecture. The dual-task output of the CNN model provides information on the direction (classification) and magnitude (regression) of the pressure in real-time.

2.2. Fabrication Process

The master mold for the sensor fabrication was designed using a 3D modeling software, followed by its production through 3D-printing using water-soluble PVA material (**Figure 2**a). Dragon skin 10 (DS10) layer was spin coated on a glass wafer as the bottom layer of the sensor (Figure 2b). After the first master mold was placed on the bottom layer, a DS10 layer was spin coated again to form the middle layer (Figure 2c,d). Following the placement of the second master mold onto the middle layer, the top layer of DS10 was spin coated as shown in Figure 2e,f and Figure S2 (Supporting Information). After curing, water was introduced to dissolve the 3D-printed PVA master molds within the Dragon Skin, resulting in the formation of empty microchannels (Figure 2g). Then, liquid metal (Galinstan) was used to fill the empty microchannels (Figure 2h). Finally, a vacuum was applied to fabricate a dome-shaped multidirectional sensor (Figure 2i–k). A comprehensive explanation of the sensor fabrication process is provided in the experimental section and dimensions in Figure S3 (Supporting Information).

2.3. Response of Fabricated Pressure Sensor

When pressure is applied to the liquid metal microchannel, its cross-sectional area is decreased and the electrical resistance is increased as a consequence (**Figure 3**a). Equation 1 describes how the microchannel's height (Δh) changes when subjected to normal stress (σ_z). On the other hand, the second equation (Equation 2) represents the corresponding relative change in electrical resistance.[31,32]

$$\Delta h = \frac{2\left(1-\nu^2\right) w \sigma_z}{E} \quad (1)$$

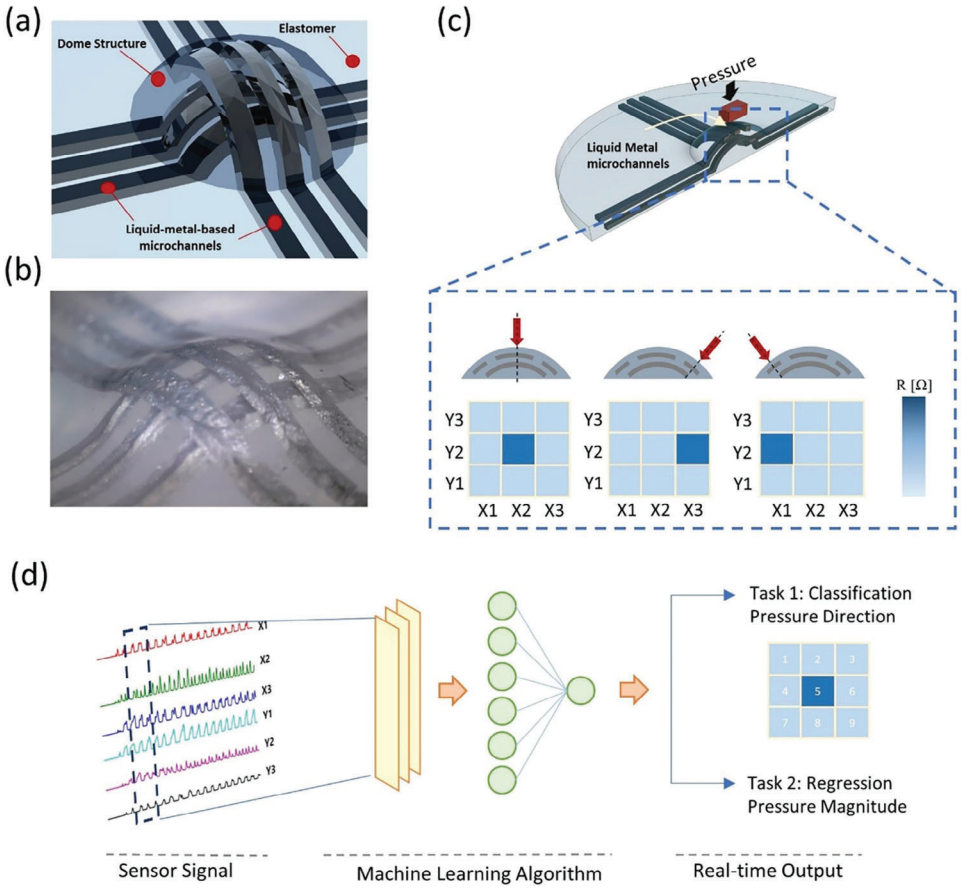

Figure 1. Overview of the liquid-metal-based soft sensor and multidirectional detection by machine learning. a) Schematic representation of liquid-metal-based soft sensor composed of dome structure, elastomer, and liquid-metal-based microchannels. b) Image of the fabricated liquid-metal-based soft sensor. c) Schematic representation of multidirectional pressure recognition by proposed liquid-metal-based soft sensor. d) Overview of the machine learning technique used to process transient responses of the liquid-metal-based soft sensor for the real-time multidirectional classification and regression.

$$\frac{\Delta R}{R_0} = \left(\frac{1}{1 - \frac{2(1-\nu^2)}{E} \chi \sigma_z \left(\frac{w}{h}\right)} - 1 \right) \tag{2}$$

The variables used in Equations 1 and 2 are as follows: w and h represent the width and height of the microchannel, respectively, ν represents Poisson's ratio, E represents Young's modulus of the elastomer, and χ is the correction factor. When the normal stress (σ_z) is applied to the elastomer, the stress magnitude diminishes along the Z direction. The correction factor χ can be described as the factor of pressure for decreasing magnitude of the applied pressure in the Z direction in relation to the increase in the elastomer thickness. The finite element analysis (FEA) simulation conducted via COMSOL was utilized to investigate the stress distribution in the soft pressure sensor. Due to the entire soft structure of the sensor, the stress is transmitted from the top layer (X-layer) to the bottom layer (Y-layer), as demonstrated in Figure 3b. The stress distribution in layers X and Y increases when pressure is applied, the corresponding decrease in resistance change can be explained by Equation 2. Theorical estimation of the correction factor χ could be solved using through Boussinesq's method as in Figure S4 (Supporting Information). Figure 3b-i,ii depicts the stress distribution on the sensor under pressures of approximately 100 and 1000 kPa, respectively. During the initial phase of pressure application (around 100 kPa), the X-layer experience deformation whereas the Y-layer is subjected to some deformation also but remains notably less deformed in comparison to the X-layer. Consequently, this leads to no substantial change in resistance in the Y-layer of the sensor. However, as the pressure increases to about 1000 kPa, both X-layer and Y-layer undergo significant deformation. An increase in the thickness of the elastomer layer impacts the correction factor χ accordingly, leading to a reduction in resistance change of the liquid-metal-based microchannels under the same applied pressure. Experimental results corroborate these findings, with the X-layer showing a higher relative resistance change than the Y-layer under the same applied pressure (Figure 3c). In addition, the resistance change in the X-layer starts at approximately 50 kPa, while the Y-layer exhibits resistance change from approximately 150 kPa, which can be attributed to the decrease in stress transmission as the elastomer layer thickness increases. Furthermore, we conducted experiments to demonstrate the behavior of the liquid metal-based pressure sensor. Figure S5 (Supporting

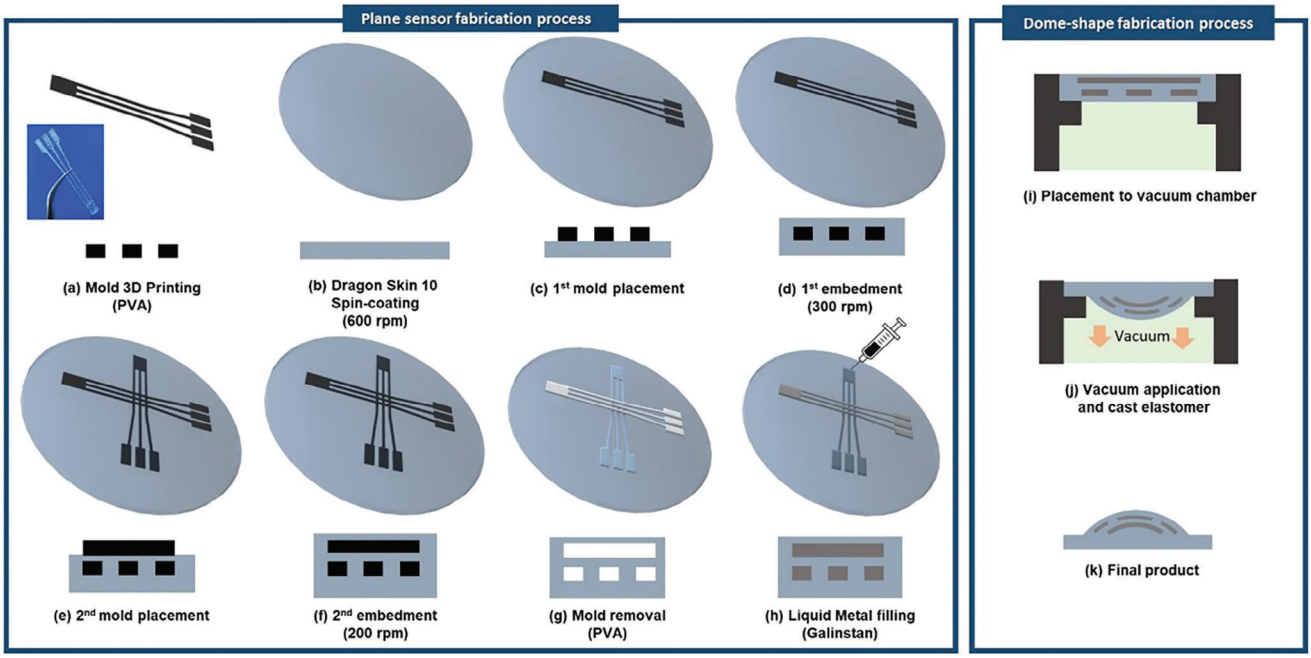

Figure 2. Fabrication process of liquid-metal-based soft pressure sensor: a) Microchannel master mold based on PVA is fabricated by 3D printer. b) Dragon Skin 10 (DS 10) layer is spin coated on a glass wafer. c) The first microchannel master mold is placed on the bottom layer. d) Additional pre-polymer is spin-coated above them as a middle layer. e) The second master mold is placed perpendicular to the first master mold. f) Additional DS 10 pre-polymer is spin-coated on the second master mold. g) PVA molds are removed by water intrusion. h) Liquid-metal (Galinstan) is injected by syringe. i) The plane sensor is placed on a vacuum chamber. j) Vacuum pressure is applied to form a concave shape and elastomer is cast and cured to generate a dome structure. k) Final sensor device is obtained.

Information) demonstrates the ability to recognize the frequency from 0.37 Hz to 1 Hz for an applied pressure of 1000 kPa. The output of the liquid metal-based pressure sensor shows a 2% change at total within the frequency range of 1 Hz to 0.37 Hz. Also, the response time of 190 ms and recovery time of 100 ms have been validated by applying 1000 kPa as illustrated in Figure S6 (Supporting Information). Moreover, the liquid metal-based pressure sensor demonstrates remarkable durability during the dynamic cycling experiment, spanning 1000 cycles (Figure S7, Supporting Information).

We observed that the liquid-metal-based pressure sensor exhibits a transient response before reaching a steady state due to its soft structure and the use of liquid metal. In Figure 3d, the transient response for each direction on the sensor is shown under multidirectional pressure application. When the pressure is applied to each sensor direction, the corresponding microchannel exhibits a change in resistance. Furthermore, Figure 3d demonstrates resistance change of directions of X1-Y1 (location 1), X2-Y2 (location 5), X1-Y3 (location 7), X3-Y3 (location 9) with matrix-based visualization of multidirectional pressure application for each direction as demonstrated in Figure 1c. When pressure is applied in the normal direction (perpendicular) to location 5, both X2 and Y2 microchannels exhibit changes in resistance. All radial directions of the sensor subjected to pressure applied at a 70° relative to the normal pressure direction to location 5. As mentioned earlier in this section, the transmitted stress decreases along the Z direction, leading to higher resistance changes in the X-layer than those in the Y-layer for all cases. Each multidirectional pressure generates a distinct transient response pattern, as observed in Figure 3d, and this feature provides the possibility of classifying the sensor output using machine learning algorithm. The detailed transient response of the sensor under varying multidirectional pressure applications can be found in Figure S8 (Supporting Information).

2.4. Classification and Regression with 1D CNN Machine Learning Algorithm

Figure 4a presents an overview of the machine learning training and real-time prediction used for monitoring multidirectional pressure. Figure 3d illustrates the transient responses of each sensor to various pressure directions, which did not saturate immediately after the pressure was applied. To achieve real-time multidirectional detection, it is crucial to classify the direction and to predict the magnitude of the applied pressure even in the transient region. Therefore, the raw data in the transient response is preprocessed by the sliding window technique and input into a 1D convolutional neural network (CNN) algorithm. The model fitting is done by training the 1D CNN. Once the prediction model is acquired, it is used for real-time prediction of multidirectional pressure. The sensor signals also require data preprocessing before input into the prediction model. Specifically, the data is segmented into sliding windows and fed into the model. The prediction model processes the segmented data and outputs the direction and magnitude of the multidirectional pressure in real time, which is displayed through a Python GUI. Figure 4b illustrates the approach used in this study for

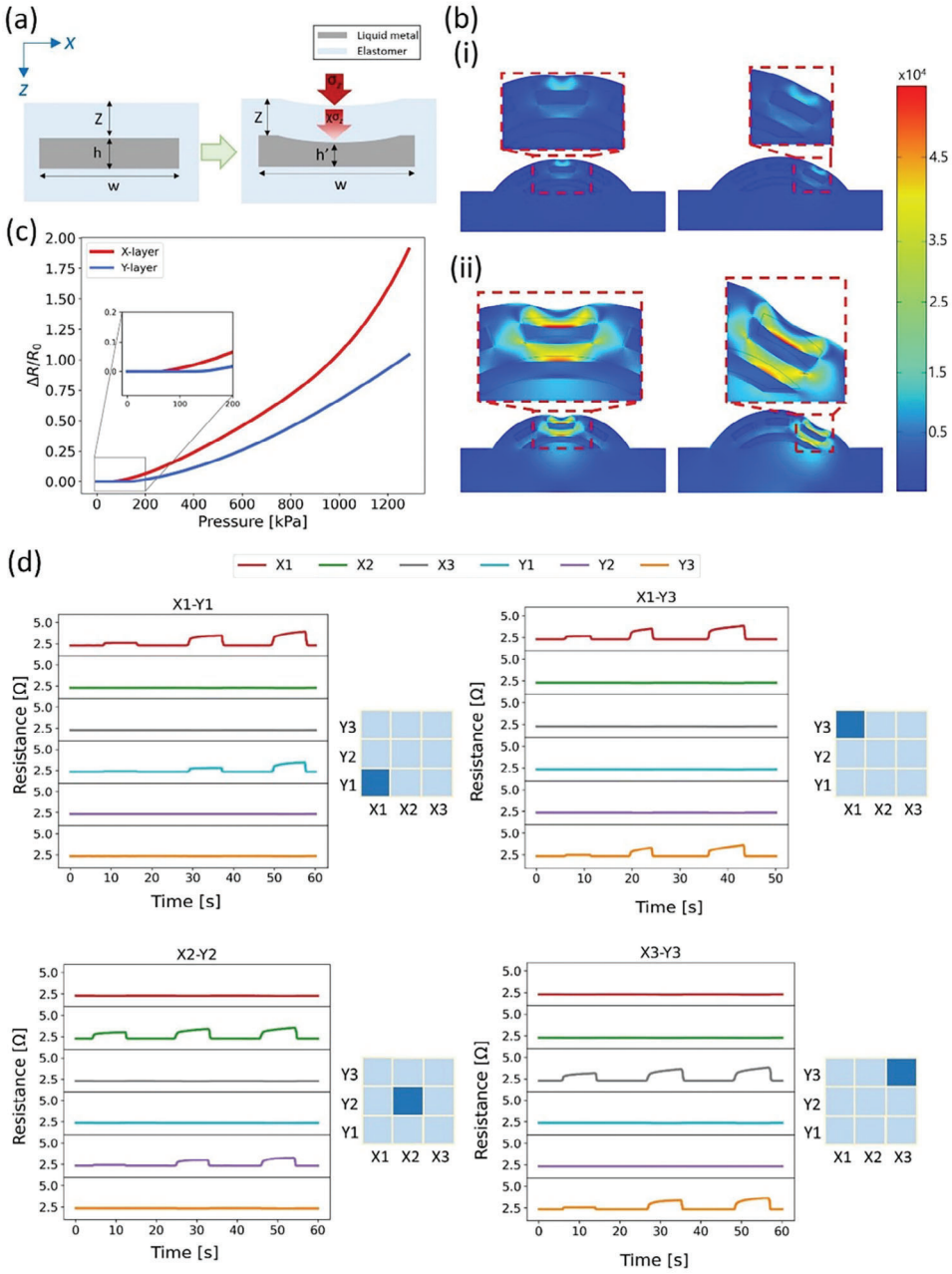

Figure 3. Responses of the liquid-metal-based soft pressure sensor. a) Schematic illustration of the sensor under pressure application. b) The finite-element analysis results in stress distribution on the sensor. (i) The stress distribution on the sensor under approximately 100 kPa for normal and directional pressure. (ii) The stress distribution on the sensor under approximately 1000 kPa for normal and directional pressure. c) Relative resistance changes of the sensor in response to applied pressure. d) Transient response of the sensor under varying multidirectional pressure applications.

identifying the direction and magnitude of the multidirectional pressure. A sliding window of 1 s was employed to capture the transient responses of all liquid metal microchannels. The microchannel responses were sampled at a frequency of 10 Hz, and after preprocessing, the sensor signals were transformed into a 1 × 4 tensor that is fed into the 1D CNN algorithm. The input data were processed through two convolutional layers with a kernel size of 3 and 1024 filters. The output of the convolutional layers was processed by a Dropout layer to prevent overfitting, followed by a MaxPooling 1D layer to reduce the dimensionality of the output. The output was then flattened and passed through fully connected layers for dual-task output. Finally, the output layer of the model consists of 10 nodes corresponding to the ten different directions of the applied pressure (including idle, meaning no pressure). Additionally, the model generates a single output for the regression (magnitude of the applied pressure). 24 cycles of training data, 8 cycles for validation, and 8 cycles for testing, which correspond to 60%, 20%, and 20%, respectively,

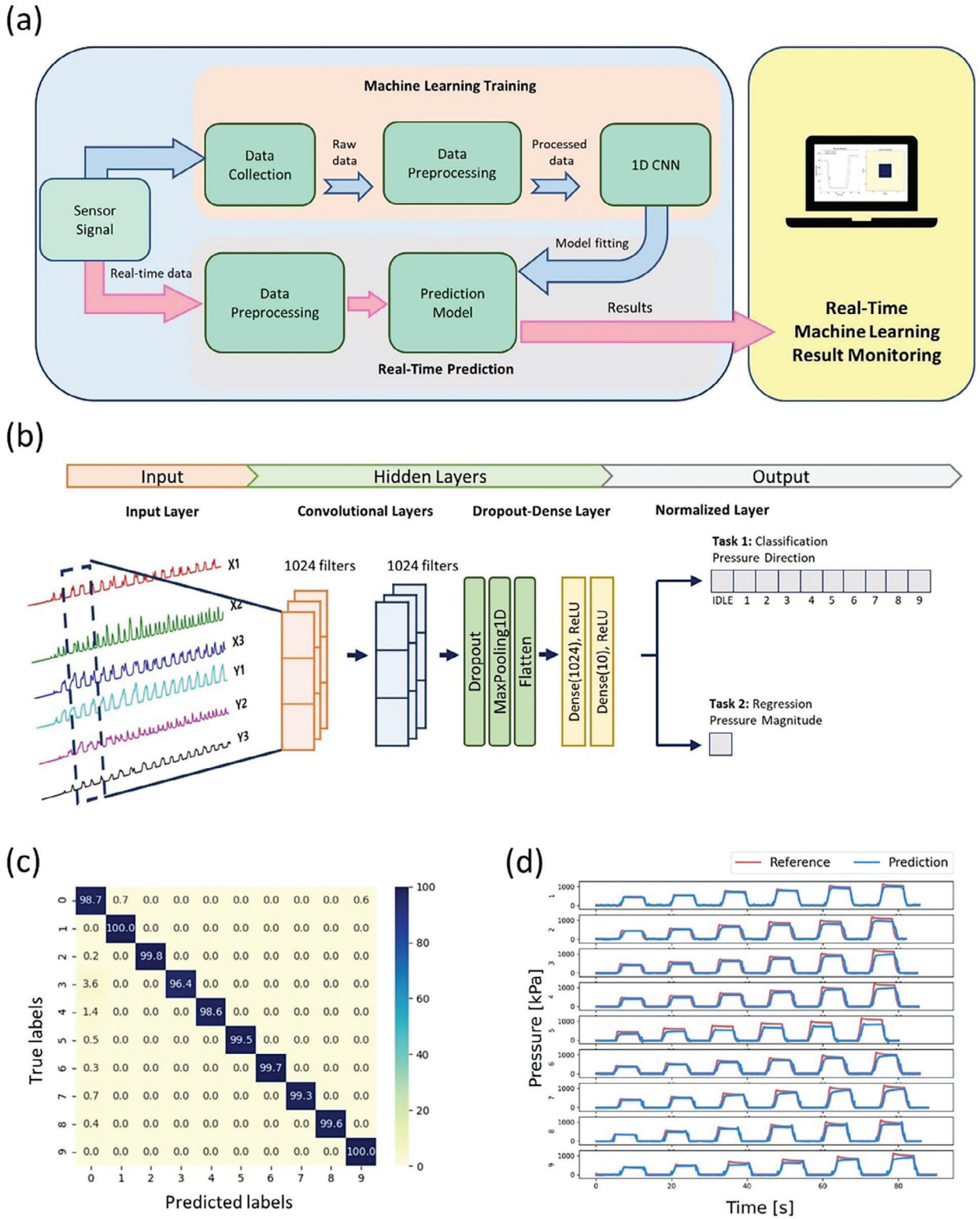

Figure 4. Classification and regression with 1D convolutional neural network (CNN) machine learning algorithm: a) Schematic diagram depicting the progression from machine learning model training to real-time predictions encompassing multidirectional classification and regression tasks. b) The CNN structure for dual-task as classification (direction of pressure) and regression (magnitude of pressure). c) Result of classification showing high classification accuracy (>96.4%) for all the ten directions (including idle), with an overall accuracy of 99.1%. d) Regression data of pressure magnitude (prediction) and measured pressure (reference).

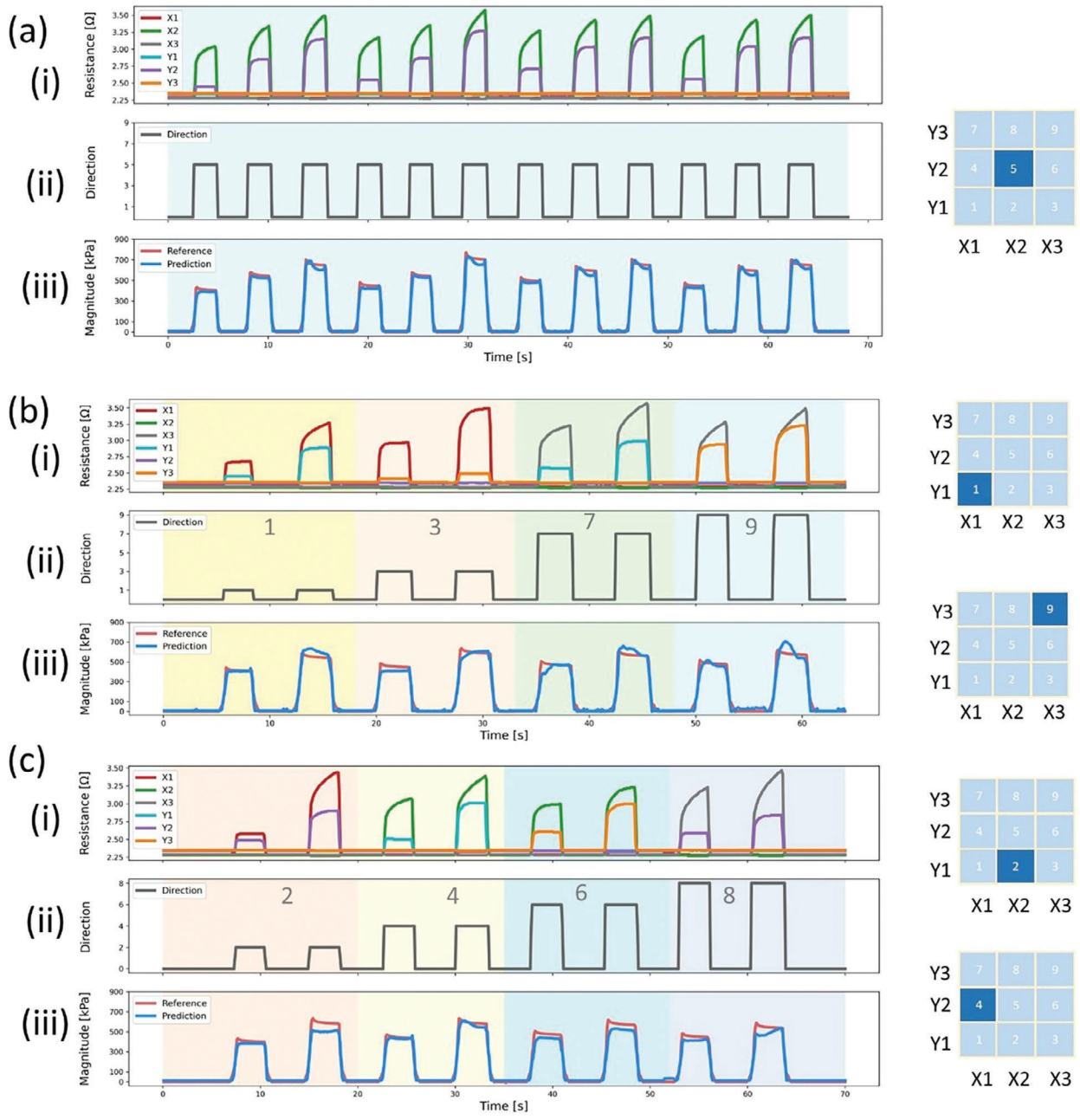

Figure 5. Real-time multidirectional pressure detection by machine learning algorithm. a) Result for normal pressure (i.e., in perpendicular direction to location #5) (i) Response of six liquid-metal-based microchannels under varying normal pressures. (ii-iii) Comparison of machine-learning-based pressure prediction and reference pressure under varying normal pressures (ii: direction, iii: magnitude). b) Results for multidirectional pressures at locations 1, 3, 7 and 9. (i) Response of six liquid-metal-based microchannels under multidirectional pressures at locations 1, 3, 7, and 9. (ii,iii) Comparison of machine-learning-based pressure prediction and reference pressure under varying directions and magnitudes of pressures (ii: direction, iii: magnitude). c) Results for multidirectional pressures at locations 2, 4, 6 and 8. (i) Response of six liquid-metal-based microchannels under multidirectional pressures at locations 2, 4, 6 and 8. (ii,iii) Comparison of machine-learning-based pressure prediction and reference pressure under varying directions and magnitudes of pressures (ii: direction, iii: magnitude).

of the overall machine learning dataset were collected. The collected machine learning data included a range of 300–800 kPa with an increment of 100 kPa for training. In the case of validation, a range of 350–750 kPa with an increment of 100 kPa data was obtained. However, for the testing data, values were randomly selected, such as 320, 430, and 570 kPa. The machine learning training results are shown in Figure 4c,d. Figure 4c displays the confusion matrix, indicating an overall classification accuracy of 99.1% and minimum classification accuracy of 96.4%. Additionally, Figure 4d shows the predicted pressure magnitude

in comparison to the reference load cell value which exhibits a regression error of 20.13%.

2.5. Real-Time Multidirectional Pressure Detection

The process of conducting real-time machine learning was depicted in Figure 4a and explained in detail in the previous section. An experiment was carried out to confirm the real-time machine learning outcomes in terms of the predicted direction and magnitude of the applied pressure. **Figure 5**a shows the prediction result of normal pressure (vertical to the sensor, i.e., perpendicular direction to location #5) from real-time machine learning. Figure 5a-i illustrates the changes in resistance of the liquid-metal-based soft sensor when varying normal pressures were applied (Video S1, Supporting Information). The experiment results indicate that the sensor can produce consistent and repeatable measurements for repeated pressure applications, which in turn leads to consistent machine learning outcomes. As shown in Figure 5a-ii, comparing the reference and predicted pressure values for normal pressure reveals a good match between them. In Figure 5b, the sensor is subjected to radial pressures applied to directions 1, 3, 7, and 9(Video S2, Supporting Information). Figure 5b-i displays the changes in resistance of the sensor for different pressure directions (i.e., radial pressure at locations 1, 3, 7, and 9). Figure 5b-ii compares the reference and predicted pressures for each direction. The liquid metal soft sensor was also subjected to radial pressures applied to locations 2, 4, 6, and 8, as shown in Figure 5c (Video S3, Supporting Information). From these results, we could confirm that the dual-task 1D CNN with the developed pressure sensor was able to successfully predict both the direction and magnitude of the applied pressure simultaneously. Therefore, this is a promising approach to detect multidirectional pressure in real-time for various applications such as wearable devices, robotics, and human–machine interfaces.

2.6. Application: Human–Machine Interface with Multidirectional Pressure Detection in Real Time

The liquid-metal-based soft sensor with multidirectional pressure detection and real-time machine-learning predictions can be used as a soft human–machine interface for controlling various devices. We demonstrate the approach using an RC model car controlled by real-time multidirectional pressure predictions. **Figure 6**a depicts the process of implementing this. The sensor signal is acquired from the sensor and then passed to the preprocessing step. Afterwards, the preprocessed data is transmitted to a real-time prediction model based on machine learning algorithm. The model generates two outputs: classification for the direction and regression for the magnitude of multidirectional pressure. These outputs are sent to the RC model car via a Bluetooth module powered by an Arduino, which receives the commands and controls the car's movement. Figure 6b demonstrates the remote controlling data generated by the liquid-metal-based soft pressure sensor and machine learning algorithm (Video S4, Supporting Information). Figure 6b-i displays the acquired raw sensor data, while Figure 6b-ii shows the predicted direction of the applied pressure. The directions of pressure on the locations of 6, 4, 2, and 8 correspond to the forward, backward, counterclockwise, and clockwise movements of the RC car, respectively (Figure 6c). Figure 6b-iii depicts the predicted magnitude of the applied pressure. The liquid-metal-based soft pressure sensor developed in this study can be used as a human-machine interface to control various devices in real-time using machine learning. Its ability to detect multidirectional pressures, along with its real-time machine-learning prediction capabilities, makes it a promising candidate for use as a human-machine interaction device in controlling a wide range of devices. Although this study demonstrated the use of the sensor in controlling an RC model car, further applications such as prosthetics, soft robotics, and entertainment devices can be realized.

3. Conclusion

In this study, we introduced a new approach for developing a multidirectional pressure sensing system using a dome-shaped 3D soft pressure sensor with multiple liquid metal microchannels and machine learning algorithm. Our research involved the application of a 1D convolutional neural network (CNN) based machine learning algorithm to analyze these transient responses of multiple liquid metal channels in order to identify both the direction and magnitude of the applied multidirectional pressures for advanced applications. The developed 1D CNN algorithm has proven effective in real-time identification of both the direction and magnitude of applied multidirectional pressures. Hence, we were able to showcase a human-machine interface application wherein the sensor was utilized to control the movement of an RC model car in real time. Overall, the developed liquid-metal-based soft pressure sensor with real-time machine-learning-based predictions holds promise for diverse applications that demand the identification of direction and magnitude of the applied pressure. These applications span across fields such as robotics, prosthetics, virtual reality, and so on.

4. Experimental Section

Materials: Dragon Skin 10 (Smooth-on, USA), Easy Release 200 (Smooth-on, USA), PVA filament (2.75 mm, Ultimaker, USA), Galinstan (Santech Materials, China) were all used as purchased.

Fabrication Process: The 3D-printed master mold was designed by a 3D computer-aided design (CAD) program (Fusion 360, Autodesk, USA). After modeling the mold, the 3D CAD file was converted to a STL file, and which was then imported into the 3D printing software (Cura 4.10, Ultimaker, USA). After 3D printing with water-soluble PVA, the master mold was carefully detached from the printing bed with a razor blade. Before the spin-coating of Dragon Skin 10 (DS10) on the glass wafer, a releasing agent (ER-200, Smooth-On Inc., USA) was coated on the glass wafer to release the elastomer easily. The pre-polymer mixture of DS10 was prepared by mixing its components, A and B, with a ratio of 1:1. The mixed DS10 was degassed in the vacuum chamber for 10 min. As the bottom layer, the glass wafer was spin-coated (600 rpm, 60s) with prepared DS10 and cured at 70 °C for 2 h. Then, the first microchannel master mold based on PVA was placed on the bottom layer, and additional pre-polymer DS10 was spin-coated (300 rpm, 60 s) above them as a second layer. After curing the second layer, the second master mold was placed perpendicular to the first master mold. Then, the additional pre-polymer DS10 was spin-coated (200 rpm, 60 s) above the second PVA master mold as the top layer and cured at 70 °C for 2 h. After curing the specimen, small holes were opened on the top layer at the ends of the molds for PVA removal.

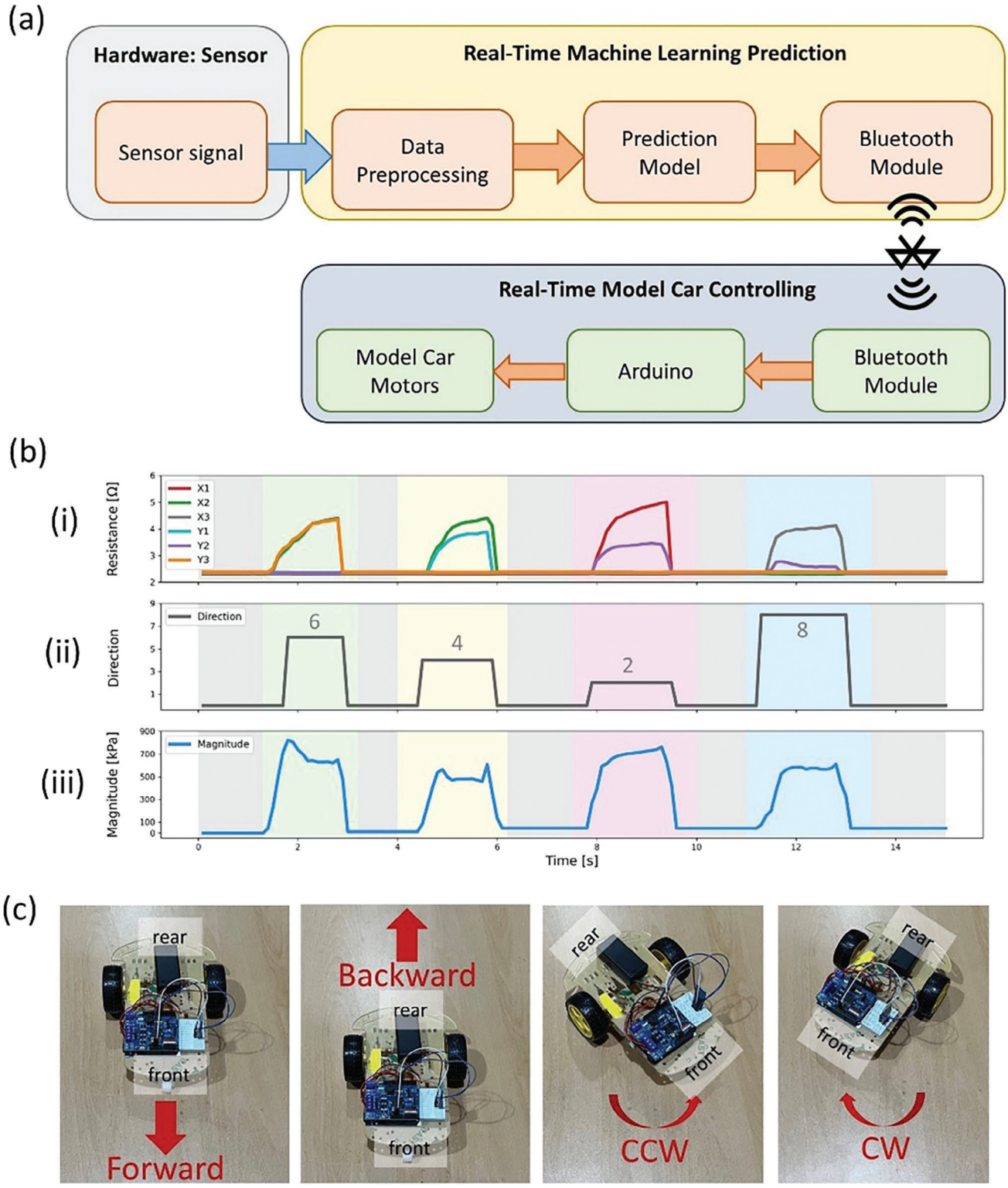

Figure 6. Demonstration of the liquid-metal-based soft pressure sensor for human–machine interface. a) Schematic diagram of real-time RC model car controlled by machine learning prediction using the liquid-metal-based soft pressure sensor. b) Demonstration of the real-time machine learning prediction of applied pressure. (i) Response of six liquid metal microchannels to sequential multidirectional pressures. (ii-iii) Result of real-time prediction of direction and magnitude of applied pressure by machine-learning algorithm c) Demonstration of the RC model car control by real-time machine-learning-based classification and regression of applied multidirectional pressure.

The sensor was placed in the deionized water at 70 °C for a day. Consecutive water intrusion was achieved by using a syringe through the holes to remove the PVA mold, resulting in the fabrication of empty microchannels. After drying the specimen at 70 °C for 30 min, galinstan was introduced into the empty microchannels through the vacuum-filling method. An additional layer of elastomer was used to seal the holes, which was applied through spin-coating at 1000 rpm for 60 s. A vacuum chamber was utilized to fabricate a 3D dome structure. The intersection area of horizontal and vertical liquid-metal-based plane sensor was positioned onto a 5 mm diameter hole. Applying a negative pressure to the plane sensor resulted in the formation of a concave hill. Under Δp = -60 kPa, the maximum height (H) of the dome was 2.1 mm when the total thickness of the plane sensor was 1.6 mm. In order to maintain the dome-shape of the liquid-metal-based soft sensor, DS10 was filled in the concave hill structure and then cured. Once the curing process was complete, the vacuum chamber was depressurized, and the final sensor structure was obtained. Finally, electrical wires were connected to the reservoirs of each microchannel.

FEA Simulation: Finite element analysis (FEA) was performed using COMSOL to investigate the deformation of the liquid-metal-based soft pressure sensor under applied normal and radial pressures. In Figure S9 (Supporting Information), the structure design of FEA simulation model for normal and radial pressure cases are demonstrated. The Dragon Skin 10 and liquid-metal were modeled as Yeoh and Neo-Hookean hyperelastic materials. The Young's modulus of the Dragon Skin 10 used for the simulation were E_{DS10} = 125 kPa.[33] The coefficients C_{10}, C_{20}, and C_{30} were 1.00×10^{-1}, 6.42×10^{-2}, 8.08×10^{-5} MPa.[34] C_{10} = 0.5 kPa was used for the coefficient of liquid-metal-based microchannels based on the shear modulus of 1 kPa.[35] To investigate the normal and radial pressure application cases by FEA simulation, the sequence type is selected as physics-controlled mesh with element size of "fine" (Figure S10, Supporting Information)

Signal Processing: The study utilized TensorFlow (version 2.7.0) as the framework for implementing the supervised machine learning technique to analyze the response of the liquid-metal-based soft sensor. The technique utilized 1D convolutional neural networks and a sliding window approach for real-time classification and regression of the applied pressure. The graphical user interface (GUI) was developed using Python's Tkinter library to monitor the sensor data and the machine learning predictions.

Human–Machine Interaction Application: The movement of the RC model car was regulated by sensor data obtained and used to adjust the machine-learning results accordingly. Sensor resistance data were acquired by connecting the sensor and a reference resistor in series to create a voltage-dividing circuit (Figure S11, Supporting Information). The application system was divided into computer and wireless communication to the RC model car. The sensor was connected to an ADS1115 converter, capable of providing a high precision of 16-bit resolution at a sampling rate of 860 samples per second over the I2C interface. The acquired sensor signals amplified and recorded by an Arduino Due were further processed using PyCharm software for machine learning analysis. After analyzing the sensor signal in PyCharm software, the results are sent from the computer's Bluetooth module to the RC model car's Bluetooth module (HC-05, Tenco Technology, USA). The motors of the RC model car are controlled by the Arduino Uno board using the machine learning predictions received via Bluetooth module.

Supporting Information

Supporting Information is available from the Wiley Online Library or from the author.

Acknowledgements

This work was supported by (1) the National Research Foundation of Korea (NRF) grant funded by the Korea government (MSIT) (No. 2021R1A2C3008742) (2) Institute of Information & Communications Technology Planning & Evaluation (IITP) grant funded by the Korea government (MSIT) (No. 2022-0-00025, Development of soft-suit technology to support human motor ability) (3) Ministry of Culture, Sports and Tourism and Korea Creative Content Agency (Project Number: R2021040018) (4) Korea Evaluation Institute of Industrial Technology (KEIT) grant funded by the Korea government (MOTIE) (No. RS-2022-00154781).

Conflict of Interest

The authors declare no conflict of interest.

Data Availability Statement

The data that support the findings of this study are available from the corresponding author upon reasonable request.

Keywords

3D printing, human-machine interaction, liquid metal, machine learning, soft sensor

Received: December 11, 2023
Revised: March 10, 2024
Published online:

[1] J. C. Yang, J. Mun, S. Y. Kwon, S. Park, Z. Bao, S. Park, *Adv. Mater.* **2019**, *31*, 1904765.
[2] J. Dargahi, S. Najarian, *Int. J. Med. Rob.* **2004**, *1*, 23.
[3] J. Hao, C. Bonnet, M. Amsalem, J. Ruel, P. Delmas, *Pflügers Arch.-Eur. J. Physiol.* **2015**, *467*, 109.
[4] A. Chortos, J. Liu, Z. Bao, *Nat. Mater.* **2016**, *15*, 937.
[5] D. H. Ho, Q. Sun, S. Y. Kim, J. T. Han, D. H. Kim, J. H. Cho, *Adv. Mater.* **2016**, *28*, 2601.
[6] N. Lu, C. Lu, S. Yang, J. Rogers, *Adv. Funct. Mater.* **2012**, *22*, 4044.
[7] T. Yu, Y. Tao, Y. Wu, D. Zhang, J. Yang, G. Ge, *Micromachines* **2023**, *14*, 716.
[8] D. Zhang, X. Wang, Y. Wu, H. Song, Z. Ma, X. Zhang, X. Yang, R. Xing, Y. Li, J. Yang, *Adv. Mater. Technol.* **2021**, *6*, 2100106.
[9] T. Q. Trung, N. E. Lee, *Adv. Mater.* **2016**, *28*, 4338.
[10] J. Yang, P. Nithyanandam, S. Kanetkar, K. Y. Kwon, J. Ma, S. Im, J.-H. Oh, M. Shamsi, M. Wilkins, M. Daniele, T.-I. Kim, H. N. Nguyen, V. K. Truong, M. D. Dickey, *Adv. Mater. Technol.* **2023**, *8*, 2202183.
[11] K. Kim, J. Choi, Y. Jeong, I. Cho, M. Kim, S. Kim, Y. Oh, I. Park, *Adv. Healthcare Mater.* **2019**, *8*, 1900978.
[12] Y. Meng, Y.-L. Park, H. Pei, D. Vogt, P. M. Aubin, E. Winchell, L. Fluke, L. Stirling, R. J. Wood, C. J. Walsh, *Int. J. Rob. Res.* **2014**, *33*, 1748.
[13] J. Yang, D. Tang, J. Ao, T. Ghosh, T. V. Neumann, D. Zhang, Y. Piskarev, T. Yu, V. K. Truong, K. Xie, Y.-C. Lai, Y. Li, M. D. Dickey, *Adv. Funct. Mater.* **2020**, *30*, 2002611.
[14] J. Xu, Z. Wang, X. Wang, Y. Wu, R. Xing, T. Yu, Y. Li, J. Ao, Y. Tao, B. Bai, M. D. Dickey, D. Zhang, J. Yang, *Adv. Mater. Technol.* **2023**, *8*, 2201193.
[15] D. Zhang, Y. Zhong, Y. Wu, X. Zhang, M. D. Dickey, J. Yang, *Compos. Sci. Technol.* **2021**, *216*, 109066.
[16] C. Liang, Y. Wu, D. Zhang, Y. Tao, T. Yu, R. Xing, J. Yang, *IEEE Sens. J.* **2023**, *23*, 5841.
[17] X. Xue, D. Zhang, Y. Wu, R. Xing, H. Li, T. Yu, B. Bai, Y. Tao, M. D. Dickey, J. Yang, *Adv. Funct. Mater.* **2023**, *33*, 2210553.
[18] C. M. Boutry, M. Negre, M. Jorda, O. Vardoulis, A. Chortos, O. Khatib, Z. Bao, *Sci. Rob.* **2018**, *3*, eaau6914.

[19] M.-S. Suen, Y.-C. Lin, R. Chen, *Sens. Actuators, A* **2018**, *269*, 574.
[20] M. Zhang, X. Gao, C. Lu, D. Yao, L. Wu, D. Li, H. Fang, S. A. Y. Sun, *ACS Appl. Mater. Interfaces* **2021**, *13*, 55735.
[21] Y. Gong, X. Cheng, Z. Wu, Y. Liu, P. Yu, X. Hu, *IEEE Sens. J.* **2021**, *21*, 21989.
[22] Kim, D., Y.-L. Park, in *2018 IEEE/RSJ Int. Conf. on Intelligent Robots and Systems (IROS)*, IEEE, Madrid, Spain **2018**, pp. 7480–7485.
[23] S. Han, T. Kim, D. Kim, Y.-L. Park, S. Jo, *IEEE Rob. Autom. Lett.* **2018**, *3*, 873.
[24] Y.-L. Park, D. Tepayotl-Ramirez, R. J. Wood, C. Majidi, *Appl. Phys. Lett.* **2012**, *101*, 191904.
[25] J.-I. Lee, S. Pyo, M.-O. Kim, J. Kim, *Nanotechnology* **2018**, *29*, 055501.
[26] S. Pyo, J.-I. Lee, M.-O. Kim, H.-K. Lee, J. Kim, *Micro Nano Syst. Lett.* **2019**, *7*, 5.
[27] Y. Jung, D.-G. Lee, J. Park, H. Ko, H. Lim, *Sensors* **2015**, *15*, 25463.
[28] Vogt, D. M., Y.-L. Park, R. J. Wood, *IEEE Sens. J.* **2013**, *13*, 4056.
[29] T. Kim, Y.-L. Park, *IEEE Rob. Autom. Lett.* **2018**, *3*, 881.
[30] K. Kim, J. Ahn, Y. Jeong, J. Choi, O. Gul, I. Park, *Micro Nano Syst. Lett.* **2021**, *9*, 2.
[31] Y.-L. Park, C. Majidi, R. Kramer, P. Bérard, R. J. Wood, *J. Micromech. Microeng.* **2010**, *20*, 125029.
[32] O. Gul, K. Kim, J. Gu, J. Choi, D. Del Orbe Henriquez, J. Ahn, I. Park, *ACS Appl. Electron. Mater.* **2021**, *3*, 4027.
[33] M. S. Xavier, A. J. Fleming, Y. K. Yong, *Adv. Intell. Syst.* **2021**, *3*, 2000187.
[34] L. Marechal, P. Balland, L. Lindenroth, F. Petrou, C. Kontovounisios, F. Bello, *Soft Rob.* **2021**, *8*, 284.
[35] Y. Qiu, Z. Zou, Z. Zou, N. K. Setiawan, K. V. Dikshit, G. Whiting, F. Yang, W. Zhang, J. Lu, B. Zhong, H. Wu, J. Xiao, *npj Flexible Electron.* **2023**, *7*, 37.